Real-time assessment of flutter stability based on automated output-only modal analysis

G. Jelicic[1], J. Schwochow[1], Y.Govers[1], A. Hebler[1], M. Böswald[1]
[1] Deutsches Zentrum für Luft- und Raumfahrt (DLR), Institute of Aeroelasticity
Bunsenstr. 10, 37073 Göttingen, Germany
e-mail: **Goran.Jelicic@DLR.de**

Abstract

During the development of new aircraft wind tunnel testing of 2D and 3D airfoils or even complete aircraft is essential. The structural integrity of the wind tunnel model needs to be assured for the test campaign because a failure can cause severe damage on the wind tunnel facility and means the loss of the costly model itself.

To enhance the level of safety, a detection of the flutter stability while testing is necessary. This paper addresses a method for fast and reliable identification of eigenfrequencies and damping ratios using operational modal analysis methods. The developed procedure has been applied in a wind tunnel test campaign by the Institute of Aeroelasticity of the German Aerospace Center (DLR) in the Transonic Wind Tunnel in Göttingen, Germany. A 2D airfoil was tested in a so-called flutter test rig with two degrees of freedom for pitch and heave motion.

The main focus of the presented method is the time efficiency of the algorithm which enables the user for quasi "real time assessment" of the flutter stability.

1   Introduction

The flutter phenomenon involves an aeroelastic structural instability which may be violent in nature (explosive flutter), and, it may therefore exhibit a rapid deterioration in modal dampings with speed increase. Experiments for aeroelastic stability in wind tunnels are made to define the flutter characteristics of models of complete aircraft or their components. Such testing necessarily entails the risk of model damage due to the destructive oscillations that can occur at flutter. This risk is reduced if the flutter onset can be predicted from the model behavior in the subcritical region below the flutter boundary. It is required to identify the vibration modes critical to flutter and to measure the damping and frequencies of these modes. They must be tracked as the test conditions are varied until a damping trend can be reliably extrapolated to a flutter condition of zero damping.

The aeroelastic interaction of a typical transport aircraft structure and the transonic flow exhibits two well-known phenomena: firstly, in the transonic dip the flutter speed shows a noticeable minimum between the critical Mach number where local supersonic regions occur in the flowfield and the Mach number where massive flow separation limits the operational flight regime [1]; secondly, amplitude-limited oscillations of the structure, so-called limitcycle oscillations (LCO), may occur instead of classical flutter where the amplitude of the structural oscillations grow exponentially at flight speeds above the critical flutter speed [2]. It is assumed in the literature that both phenomena are linked to the inherently nonlinear aerodynamics at transonic speeds. Since the relative flow speeds are close to the speed of sound, shock waves occur which may interact with the boundary layer eventually leading to flow separation. All of these mutual interactions are sources of nonlinearities. As mentioned above the damping and frequency trends of the flutter experiments in the Transonic Wind Tunnel in Göttingen (TWG) must be monitored to approach the unstable boundary in a safely manner, which requires quasi "real time assessment" of the flutter stability during operation.

In the last years, different system identification methods were developed to perform automatic modal analysis based only on the structural response of buildings and vehicles under ambient excitation. This so-called operational modal analysis methods (OMA) try to approximate directly the time domain response, e.g. data-driven stochastic subspace identification (SSI,[5][8]), or the cross power spectral densities CPSD in frequency domain using rational polynomials, e.g. least-square complex frequency estimator (LSCF,[6]) or poly-reference LSCF (pLSCF,[7]). Several time domain methods use the cross correlation functions, which are the inverse Fourier-Transforms of the CPSD, e.g. NExT-LSCE [3], NExT-ERA [4] or covariance-driven SSI [8].

In this study, the modal characteristics of the aeroelastic airfoil model must be obtained during *operation* in the TWG in order to observe its interaction with airflow. For in-flight or wind gallery tests it is desirable to monitor the evolution of the system's eigenfrequencies and damping as operating conditions are being modified. In the following the implementation of the well-known LSCF identification method is presented, which runs very rapid and without user interaction.

2   Aeroelastic system identification

Real-time automated modal analysis describes a procedure by which time data is continually collected, processed and automatically analyzed to identify the modal parameters of a structure.

Though "real-time" may be a misnomer because a certain data sample must first be collected before it can be analyzed, modal analysis forms a prediction of the system's behavior based on its dynamical characteristics, thus allowing to foresee, for example, the onset of an unstable state. Trending of time data reveals instabilities when the system already is in an unstable state.

In experimental modal analysis (EMA) excitation and response of a system are both measured and their relationship evaluated in time or frequency domain as the system's transfer function. Numerical identification will find a mathematical model which approximates the transfer function.

If ambient excitation cannot be measured or eliminated, only vibration responses are acquired. Without knowledge of the excitation forces quantitative information about the cause of the vibration is missing, therefore the methods of OMA must be employed. Unlike experimental modal analysis, the frequency response function (FRF) cannot be estimated and the primary data source for modal identification become the CPSD calculated between response sensors and reference sensors. This renders calculation of the modal mass impossible and results in a higher stochastic variance and lower data quality, but eigenvalues and eigenmodes can still be identified.

In order to collect enough information about a system, the data sample must have a certain sampling frequency and acquisition time. The sampling frequency is set by the maximal frequency of interest for the modal analysis, the frequency resolution by the number of data points needed for convenient estimation of modal parameters.

Sampling frequency relates to the maximal practically measurable frequency of a system ($f_{max} = f_s/2$) and acquisition time to frequency resolution ($\Delta f = 1/T_s$), delivering $N_s = f_s T_s/2$ data points in the frequency domain.

Noise levels must be reduced in order to diminish the bias on the measured parameters because several identification algorithms are not efficient and consistent [11][16]. A window function of size $N<N_s$ reduces data noise by averaging over many data blocks, but increases frequency resolution linearly by a factor N_s/N, thus forcing a longer acquisition time in order to satisfy a minimum Δf requirement.

The demands of noise reduction and the requirement of identifying a certain frequency range impose the time delay between data acquisition and system identification. The available computation speed only determines how often data can be analyzed.

Time data is acquired in blocks of length $N_B = T_A/f_s$ dictated by the available analysis (computation) time T_A before a new block arrives. Many blocks are then stacked in a dynamic first-in-first-out buffer whose size depends on the required frequency resolution.

2.1   Theory

Several algorithms handle large and noisy data sets in frequency domain from modal analysis tests containing multiple sensors and multiple exciters. The LSCF estimator is described in this text with some insights on computational complexity and comparisons with the poly-reference pLSCF estimator.

The order of magnitude of computation time is presented for typical practical cases using the authors' mobile computer as reference (i7 Intel, 8GB RAM, SSD, year 2013).

LSCF identifies the modal characteristics of a dynamic system by estimating polynomial coefficients and then directly from them the poles and modal participation factors using a common denominator formulation describing the transfer function.

For a multiple inputs – multiple outputs linear, time invariant system, with N_o sensors (outputs) and N_i exciters (inputs), the transfer function matrix entries can be represented as a rational polynomial of order N_p as function of the complex frequency s:

$$H_{oi}(s) = \frac{\sum_{n=0}^{N_p} b_{n,oi} s^n}{\sum_{n=0}^{N_p} a_n s^n} \quad \in \quad \mathbb{C}^{N_o \times N_i} \tag{1}$$

The LSCF algorithm estimates the coefficients a_n and $b_{n,oi}$, from which then the poles and zeroes of the transfer function can be calculated as polynomial roots. There are different implementations of LSCF that identify the system each with different asymptotic properties in the least-squares (LS), total least-squares (TLS), generalized total least-squares (GTLS) and maximum likelihood (ML) senses [14]. The limited time available for identifying the system restrains the applicability of iterative and poly-reference methods for the *real-time automated modal analysis*.

For a stationary stochastic process, the power spectra $S_{yy}(s) \in \mathbb{C}^{N_o \times N_o}$ of the outputs are given by:

$$S_{yy}(s) = H(s)S_{ff}(s)H(s)^H \tag{2}$$

with $S_{ff}(s) \in \mathbb{C}^{N_i \times N_i}$ the cross-power spectral densities of the unknown input forces. Assuming white noise exciting the system, S_{ff} is constant with respect to frequencies:

$$S_{yy}(s) = H(s)H(s)^H |S_{ff}|, \quad |S_{ff}| = const. \tag{3}$$

The eigenvalues and eigenmodes of the system can be identified, although the missing information about exciting forces renders determination of the modal participation factors, i.e. modal scale factors, impossible. The cross power spectral density function is estimated using the periodogram approach (Welch's estimator). The double-sided cross-power spectral density of responses y with references x for each frequency k and block b are given by:

$$S_{xy}(\omega_k) = \frac{1}{N_b} \sum_{b=1}^{N_b} Y_{b,k} X_{b,k}^H \quad \in \quad \mathbb{C}^{N_y \times N_x} \tag{4}$$

with Y and X the windowed spectra of respectively responses and references. The choice of number and length of blocks affects respectively the bias and variance of the estimated power spectra.

The entire CPSD matrix is calculated at once by taking advantage of symmetry, vectorization and indexing. The FFT algorithm has $\mathcal{O}(N \log N)$ time complexity and evaluates all $N_y N_x$ spectra in parallel; overall computation time is inversely proportional to the window size and directly proportional to overlap. The N_b element-wise products of the response and reference spectra require then each $N_y N_x N$ operations. This step is economical since the data buffer is always much smaller than during EMA. The double-sided cross-power spectral density matrix can be reshaped by stacking its responses and references. Rational polynomials in the Laplace-domain can represent the system experimentally determined along the imaginary axis in the complete complex domain:

$$S_{yx}(\omega_k) \in \mathbb{C}^{N \times N_y \times N_x} \xrightarrow{\text{reshaped}} S_r(s) = \frac{\sum_{n=0}^{N_p-1} b_{n,r} s^n}{\sum_{n=0}^{N_p-1} a_n s^n} \in \mathbb{C}^{N \times N_y N_x} \tag{5}$$

with N_p defined for convenience as the highest polynomial order plus one.

The unknown coefficients a_n and $b_{n,r}$ are found by solving the so-called reduced normal equations:

$$J^H J \theta = 0 \qquad (6)$$

where $J^H J$ is the system's reduced Jacobian matrix and the parameters θ are the stacked polynomial coefficients:

$$\theta = \{\beta_1 \quad \beta_2 \quad \cdots \quad \beta_{N_y N_x} \quad \alpha\}^T \text{ with: } \beta_r = \{b_{r,1} \quad \cdots \quad b_{r,N_p}\}^T, \alpha = \{a_1 \quad \cdots \quad a_{N_p}\}^T$$

The vector α contains all denominator coefficients and the vector β_r all numerator coefficients of the CPSD's r-th column, while $J^H J$ can be rewritten as:

$$\begin{bmatrix} M_1 & \cdots & 0 & Q_1 \\ \vdots & \ddots & \vdots & \vdots \\ 0 & \cdots & M_{N_y N_x} & Q_{N_y N_x} \\ Q_1^H & \cdots & Q_{N_y N_x}^H & \sum_r^{N_y N_x} T_r \end{bmatrix} \begin{Bmatrix} \beta_1 \\ \vdots \\ \beta_{N_y N_x} \\ \alpha \end{Bmatrix} = 0 \qquad M, Q, T \in \mathbb{C}^{N_p \times N_p} \qquad (7)$$

The entries (p,q) of the $N_y N_x$ reduced matrices M, Q and T can be expressed as:

$$M_{r(p,q)} \stackrel{\text{def}}{=} \sum_{k=1}^N W_{r,k} z_k^{p-q}$$

$$Q_{r(p,q)} \stackrel{\text{def}}{=} \sum_{k=1}^N -W_{r,k} S_{r,k} z_k^{p-q} \qquad (8)$$

$$T_{r(p,q)} \stackrel{\text{def}}{=} \sum_{k=1}^N W_{r,k} S_{r,k} \overline{S_{r,k}} z_k^{p-q}$$

with W a weighting function in the frequency-domain. A poly-reference algorithm like pLSCF calculates analogously N_y reduced matrices of size $\mathbb{C}^{N_x N_p \times N_x N_p}$. It can be observed that these matrices are Hermitian and have a Toeplitz structure, therefore only one row or column need be calculated to reconstruct the whole matrix since both S and W are even functions and z is evaluated over the unit circle. Computation time is further reduced by calculating in parallel the first N_p terms of the discrete Fourier transform.

Carrying out the matrix multiplication of the above, one obtains:

$$\beta_r = -M_r^{-1} Q_r \alpha \text{ and } D\alpha = 0 \qquad (9)$$

where D is the so-called reduced Jacobian matrix:

$$D \stackrel{\text{def}}{=} \sum_{r=1}^{N_y N_x} T_r - Q_r^H M_r^{-1} Q_r \in \mathbb{C}^{N_p \times N_p} \qquad (10)$$

Time complexity for matrix multiplication and matrix inversion is somewhat lower than $\mathcal{O}(n^3)$, thus will computation time for LSCF increase as $\mathcal{O}(N_y N_x N_p^3)$; pLSCF will similarly calculate $D \in \mathbb{C}^{N_x N_p \times N_x N_p}$ by summing N_y terms [16], being thus $\mathcal{O}(N_x^2)$ slower. The reduced matrices are calculated in linearithmic time for both cases. An overview of the computational aspects of the reduced Jacobian matrices is given in [15].

Assuming conservatively a spectrum of tens of thousands frequency points and hundreds of responses and reference channels, the three reduced matrices are calculated in less than one second.

In order to remove the parameter redundancy and calculate unstable poles, $a_0 = 1$ is imposed [16], therefore the least-squares solution of the reduced normal equations for every order n is:

$$\alpha_n = \begin{Bmatrix} 1 \\ -D_{(1:n+1,2:n+1)}^{-1} D_{(1:n+1,1)} \end{Bmatrix} \in \mathbb{C}^{(n+1)\times 1} \qquad n = 1:N_p - 1 \qquad (11)$$

The complexity of this pseudoinverse is about $\mathcal{O}(N_p^3)$ in the worst case; the pLSCF version computes $\alpha \in \mathbb{C}^{N_x N_p \times N_x}$ [16].

The complex poles of the system can be calculated by finding the roots z_m of the denominator polynomial in the z-domain using the eigendecomposition of the companion matrix of vector α_n for a model order n.

$$\sum_{i=0}^n a_i s^i \xrightarrow{roots} a_n \prod_{i=1}^n (s - z_i) \xrightarrow{z=e^{\lambda \Delta t} e^{i\varphi}} \lambda_{i,n} \qquad (12)$$

The eigenvalue decomposition requires $\mathcal{O}(N_p^3)$ operations in the worst case. LSCF calculates the roots of the polynomial with coefficients $\alpha \in \mathbb{C}^{N_p \times 1}$, pLSCF similarly builds a companion matrix from $\alpha \in \mathbb{C}^{N_x N_p \times N_x}$ and calculates its eigenvalues [16].

The stabilization diagram is constructed by repeating the last two steps for many model orders down from N_p–1. The vast majority of the calculated roots are purely mathematical poles; the physical poles of the system are found by imposing:

$$\begin{aligned} \mathfrak{I}(\lambda) > 0 & \qquad \text{eigenfrequencies must be positive} \\ 0 < -\mathfrak{R}(\lambda) < |\lambda| & \qquad \text{the system must be underdamped} \end{aligned} \qquad (13)$$

At the end of this step, for each model order n, $N_m(n)<n$ physical poles are known, therefore a clean stabilization diagram can be plotted. Conservatively calculating all poles up to model order one hundred lasts tenths of a second per frequency band.

The residues of the system are determined using the Least Squares Frequency Domain (LSFD) method applied on the physical poles of the system for all (or some) model orders.

The modal decomposition of the cross-power spectral density is:

$$S(s) = \sum_{m=1}^{N_m} \left(\frac{R_{m,1}}{s - \lambda_m} + \frac{\bar{R}_{m,1}}{s - \bar{\lambda}_m} + \frac{R_{m,2}}{\bar{s} - \lambda_m} + \frac{\bar{R}_{m,2}}{\bar{s} - \bar{\lambda}_m} \right) - \frac{L_R}{s^4} + U_R \quad \in \mathbb{C}^{N \times N_y N_x} \qquad (14)$$

with

$$R_{m,1} = \psi_m L_m^T, \quad \bar{R}_{m,1} = \bar{\psi}_m L_m^T, \quad R_{m,2} = L_m \psi_m^T, \quad \bar{R}_{m,2} = \bar{L}_m \psi_m^T \qquad (15)$$

where each residue matrix $R_m \in \mathbb{C}^{N_y \times N_x}$ is the product of mode shapes ψ_m and operational reference vectors L_m^T. The upper and lower residuals U_R and L_R account for the effects of the modes outside the current frequency band. Since the poles are already known, a linear least-squares problem in the parameters R, U_R and L_R must be solved:

$$[S] = [A][X] \xrightarrow{\text{solve}} [X] = [A]^+[S] \qquad (16)$$

where $A \in \mathbb{C}^{N \times (N_m+2)}$ contains the various known $[1/(s - \lambda_m) \quad \cdots \quad -1/s^4 \quad 1]$ terms, S the measured cross-power spectral density matrix and $X \in \mathbb{C}^{N_y(N_m+2) \times N_x}$ the unknown stacked residue matrices and upper and lower residuals. This requires about $\mathcal{O}(N(N_m + 2)^2 + 2(N_m + 2)^3)$ operations.

The mode shape ψ_m corresponding to the m-th eigenfrequency are obtained using singular value decomposition of the m-th residue:

$$R_m = U_m \Sigma_m V_m^T \qquad (17)$$

The first column of the left-singular vectors U_m represents the mode shape ψ_m. At the end of this step, a mode shape of the system is known for each pole. The complexity of the two-step singular value decomposition algorithm is about $\mathcal{O}(N_y N_m^2 + N_m^3)$ [17]. Calculating the mode shapes is inexpensive: conservatively assuming one hundred modes and a thousand sensors requires one tenth of a second, though the number of modes per frequency band never exceeds a few dozens.

At this point of the identification, a mode set is available for different model orders or time instants, though relationships between each are not immediately known thus requiring *tracking* of the modes; as poles disappear or reappear due to noise or errors, relating poles with each other by simply monitoring frequency change is not practical. Tracking modes between different model orders allows to clean the stabilization diagram and to select the optimal eigenvalue and thus mode shape, whereas tracking between time instants allows to monitor system parameters changes or arising of instabilities.

The tracking algorithm evaluates the consistency (degree of linearity) between successive mode shape sets using the modal assurance criterion (MAC) matrix and calculating concurrently a number of quality parameters: mode indicator function (MIF) [12], mean phase deviation (MPD) and modal phase collinearity (MPC) [13]. By application of these indicators crossing, close or disappearing modes can be separated correctly from each other. Eigenvalues and eigenmodes identified over different model orders or instants belonging to the same physical mode are iteratively recognized as related and sorted together, after which stochastic, lone and badly identified modes are spotted and removed.

The tracking algorithm works with a variable number of modes and mode sets, and the number of operations required varies linearly with model order or time sets. The time complexity of the tracking algorithm is that of matrix operations since sorting algorithms have lower linearithmic complexity. The difficulty of tracking very much depends on the tracking criteria and how clear mode sets are.In practical cases, selecting, sorting and tracking thousands of modes requires less than a tenth of a second.

Tracking does not per se identify more precisely physical modes of the system, but instead recognizes modes as they appear or disappear in a data set and sorts them together.

2.2   Overview of time complexity

The conversion of time data into frequency domain (4) is performed rapidly as discussed earlier; this step is common for all frequency-domain identification algorithms.

Overall performance of the identification algorithm is most sensitive to the model order when calculating many times the denominator's coefficients in order to construct a stabilization diagram.

Calculation (performed once)	LSCF	pLSCF	Operation
Construct reduced Jacobian matrix (10)	$\mathcal{O}(N_y N_x N_p^3)$	$\mathcal{O}(N_y N_x^3 N_p^3)$	Matrix multiplication and inversion
Solve normal equations (11)	$\mathcal{O}(N_p^3)$	$\mathcal{O}(N_x^3 N_p^3)$	Matrix pseudoinverse
Calculate denominator's coefficients (12)	$\mathcal{O}(N_p^3)$	$\mathcal{O}(N_x^3 N_p^3)$	Eigendecomposition of companion matrix

Table 1: Time complexity of LSCF and pLSCF: comparison of slowest steps

After poles have been identified, residuals and mode shapes are calculated according to eq. (16) and (17). The tracking step employs an iterative searching and sorting algorithm which operates on problems without predetermined size or fully predictable characteristics, therefore is inherently slower than other steps, with cubic complexity with respect to number of modes and linear with respect to number of mode sets, but since the problem size is in any case small, it does not reduce much the overall speed.

2.3   Overview of MATLAB implementation

The identification algorithm is almost entirely vectorized and features minimal use of loops and conditional statements. The parallel processing toolbox is not used for the sake of portability, though MATLAB automatically switches to multiple CPU cores for intensive operations (`fft`, `eig`, `svd`, …), thus positively affecting computation time. A number of default functions have been rewritten (`repmat`, `unique`,…), along the use of undocumented functions (`ismembc`,…) and compilation of some MEX files. The algorithm evaluates user inputs and balances matrix size with number of operations to achieve fast computation. The GUI's CPU time is negligible compared to mathematical operations.

3   Test setup

The present wind tunnel investigation was carried out in the *Transonic Wind Tunnel Göttingen DNW-TWG* shown in Figure 1, which is operated by the foundation German–Dutch Wind Tunnels. The DNW-TWG is a continuously operating facility with a *1×1 m* adaptive test section. The stagnation temperature in this wind tunnel is kept constant by a closed-loop control of a cooler, while Mach number and stagnation pressure may be varied independently. A given inflow Mach number is also kept constant by a closed-loop control using the measured ratio of the static pressure to the stagnation pressure in the test

section. The ratio of the wind tunnel height to the chord of the investigated airfoil model is 3.333. The top and bottom walls were adapted to the stationary flow at the mean angle of attack of the airfoil, where the static aeroelastic equation must be satisfied.
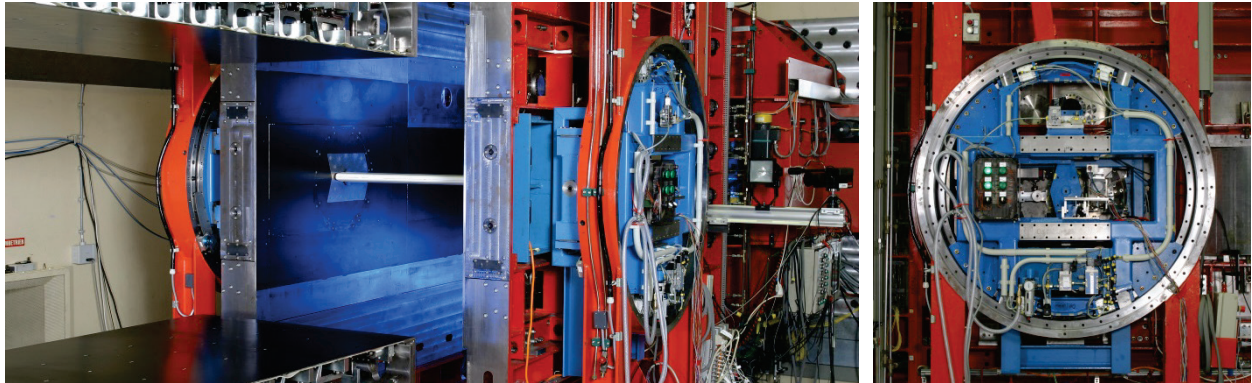

Figure 1: Test plenum of Transonic Wind Tunnel Göttingen TWG

3.1   Flutter test setup

The applied setup allows free heave and pitch motions of the airfoil model for flutter tests. A theoretical model representing the structural dynamics of this set-up is described in Figure 2. The mean angle of attack of the aeroelastic system under air loads depends on the structural dynamics parameters, the off-wind angle of attack and the flow parameters.

The entire flutter test setup can be rotated around the elastic axis of the aeroelastic system in order to tune the angle of attack to a given value while the wind tunnel is functioning, thus a target mean angle of attack can be achieved while fulfilling the static aeroelastic equilibrium.

In the flutter test setup, the airfoil is mounted on each side to a piezoelectric balance with high stiffness in order to measure the steady and unsteady lift, drag and pitching moment. Two laser triangulators on each side of the wind tunnel measure the instantaneous heave and pitch of the model. A digital signal processing device derives the heave velocity from the triangulators' signals such that a proportional voltage can be passed to an electrodynamical exciter on each side. Small heave motions of the airfoil can then either be amplified or damped, by applying the inverted signal. Tests revealed that in the open-loop state this flutter control system is unintrusive.
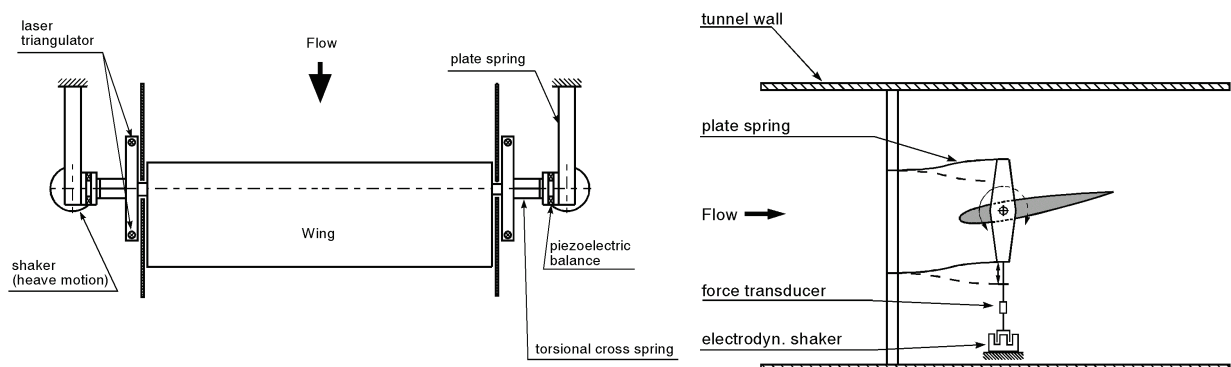

Figure 2: Model of the structural dynamics and test setup in the wind tunnel

3.2   Airfoil model

For the investigation a two dimensional model with the Dornier CAST 10-2 airfoil is used. It has a chord length of $c = 0.3\ m$ and a span of $b = 0.997\ m$. The model is made of two CFRP half shells, each having a constant spanwise laminate lay-up, with a thickness of up to $3\ mm$; the stiffness of the model is increased by a CFRP c-spar at a position of $x/c = 0.33$. At both ends, aluminium connectors, used to mount the model on the test rig, are glued to the half shells and allow oscillations about the quarter chord. Laminar-turbulent boundary-layer transition was tripped at 7.5% chord on the both sides of the airfoil. The overall weight including all movable components is $12.55\ kg$ and the inertia mass with respect to rotation axis results to $0.07\ kg{\cdot}m^2$. A flat spring and torsion spring allow heave movement and pitch rotation, respectively. There are lever arms outside of the measurement chamber, where electromagnetic shakers operate to excite the heave movement or to suppress oscillations by introducing forces with inverted phase delay. Additional balance masses can be installed on the lever arms to shift the center of gravity.

In order to measure the unsteady motion of the laminar-turbulent transition, the model was equipped with 26 hot-film sensors to determine the condition of the boundary layer. Moreover it contains 60 unsteady pressure sensors to measure the pressure distribution in a representative section. The model is equipped with six internal accelerometers (PCB 352C22) measuring perpendicular to the wing plane, and installed at $y/b = 0.15, 0.50, 0.85$ in spanwise direction and at $x/c = 0.0833, 0.8733$ in the direction of the flow. It is lightweight and very stiff so that the natural frequencies of the flutter test setup and the flutter frequencies are well below the first deformation natural frequency of the airfoil model.

4   Monitoring of flutter experiment

During the monitoring of the airfoil model, the incoming time signal blocks are continuously analyzed to identify the poles and mode shapes of the aeroelastic system as function of the current flow condition.

Measurements were conducted in the Mach number range between $0.5 \leq Ma \leq 0.85$ with control accuracy $\Delta Ma = 0.001$ and at static pressures of $40\ kPa \leq p_0 \leq 90\ kPa$ resulting in Reynolds numbers of $1.0{\cdot}10^6 \leq Re \leq 3.5{\cdot}10^6$. Since the evacuation of the chamber takes time, the static pressure is held constant during one measurement series, while the flow rate is increased in steps from minimum Mach number to maximum. Before each measurement point is recorded, the adaptive walls of the test section are adapted to the streamlines to minimize the flow effects of the wind tunnel walls. This procedure is automated and takes only a few seconds. In addition to the flow conditions the support of the model can be rotated to change the angle of attack. In total three parameters can be modified to control the flow conditions: static pressure p_0, Mach number M_∞, mean angle of attack α of the model support.

This instrumentation allows identification of the rigid body heave and pitch mode, but also several flexible bending and torsion modes at higher frequencies. In Table 2 the results of the modal survey without wind are summarized with frequencies, dampings and mode shapes.

In Figure 3 the average pressure distribution for pitch oscillation are plotted for $M_\infty = 0.5$ and $M_\infty = 0.8$ measured by the internal pressure transducers. The red and blue lines represent the pressure coefficient at fixed angle of attack, while the grey shaded region is the envelope for the unsteady pressure enforced by a pitch excitation with fixed amplitude. From the characteristics of the curves it is observable that the resulting lift force will shift from front to rear dependent on the flow velocity, caused by the rear loading effect of pressure distribution at higher Mach numbers. Since the rotation axis and the center of gravity are fixed at $1/4$ chord, the resulting aerodynamic moment will change sign at a certain Mach number from nose-up to nose-down. This aerodynamic behavior is nonlinear and is the reason, why monitoring of the flutter experiment with online system identification is required.

For the current investigation it is assumed that a classical aeroelastic instability with two degrees of freedom might occur by coupling of the heave and pitch modes. On the other hand, flutter of the pitch mode might arise because of the indifferent equilibrium of the aerodynamic loading with respect to the

rotation axis. To eliminate boundary layer effects, the transition of the flow around the airfoil was enforced by installation of a turbulator strip at the leading edge.

It is assumed that the flow's vorticity and turbulence possess sufficient random characteristics to excite all relevant modes of the aeroelastic system. In the following figures, a series of measurements points at $p_0 = 60\ kPa$ in the range of fluid speed of $M_\infty = 0.5 - 0.82$ at zero angle of attack is presented in detail. The model is mass-balanced to the rotational axis by two masses installed on the lever arms.
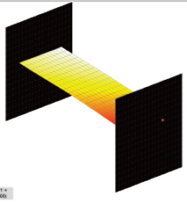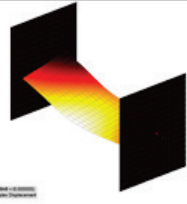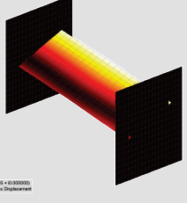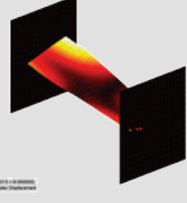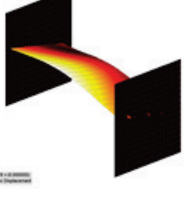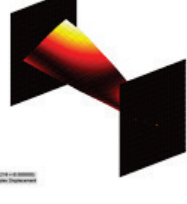
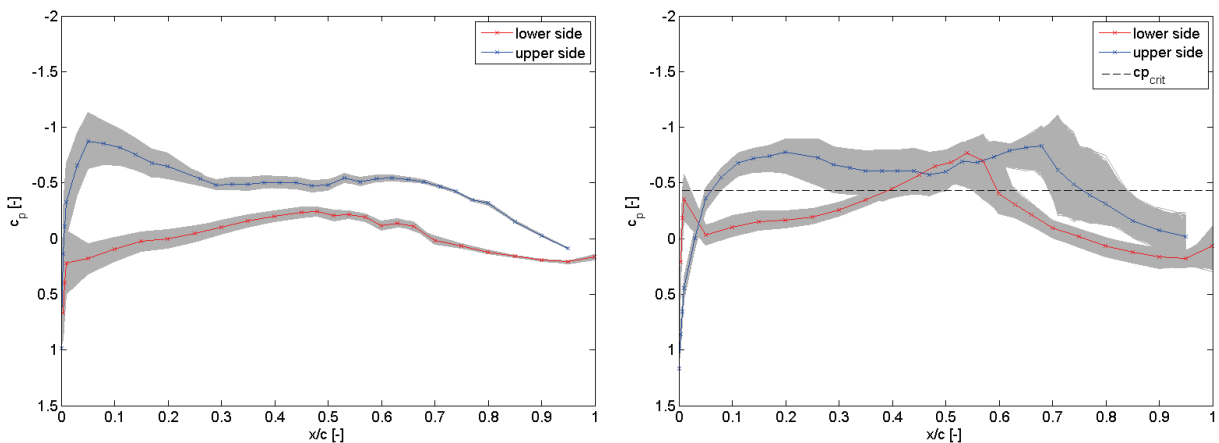| Mode	f [Hz]	d [%]	Shape	Mode	f [Hz]	d [%]	Shape
Heave	28.5	1.2		1st sym. bending	92.7	0.7	
Pitch	41.2	2.1		1st antisym. bending	109.5	0.3	
In-plane bending	90.3	0.8		Antisym. torsion	117.2	1.1	

Table 2: Mode shapes of wind tunnel model

Figure 3: Unsteady pressure distribution with free transition at $M_\infty = 0.5$ (left), $f = 4.5\ Hz$, $\alpha = 1° \pm 1°$ and $M_\infty = 0.8$ (right), $f = 7.2\ Hz$, $\alpha = 0.1° \pm 0.6°$

4.1 Implementation

A *Dewetron* measurement system [18] records all pressure, force, and acceleration signals with a sampling frequency of *4000 Hz*. The DNW-TWG *AMIS III* data acquisition system is capable of sampling up to

1024 channels simultaneously at up to *204.8 kHz* per channel and with *24 bit* resolution. The measurement system allows direct remote access to networked clients running *Dewesoft*. The automated identification algorithm running on a networked notebook in MATLAB accesses the accelerometers' signals via a DCOM interface with the *Dewesoft* client application. The basic data flow is presented in Figure 4 while a GUI of the developed MATLAB software is shown in Figure 5.

MEASUREMENT SYSTEM   NETWORKED PC

| Master Dewesoft | —*LAN*— | Client Dewesoft | —*DCOM*— | MATLAB |

data acquisition   remote access   automated identification
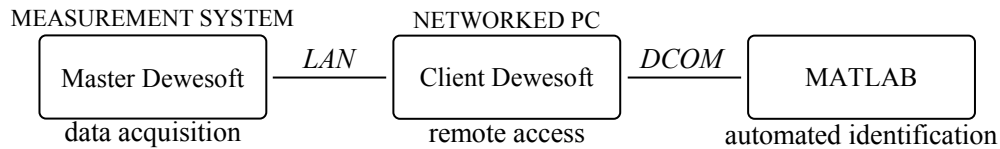
Figure 4: Diagram of automated system identification

The primary data source for identification are the CPSDs calculated from the last sixteen blocks of *4096* samples each. The program updates with each new data block (about every second). The user can select on-the-fly the identification algorithms (LSCF, pLSCF, SSI time and covariance-based SSI), and displayed synthesized spectra. The identified eigenvalues and eigenmodes are used to construct the stabilization diagram and display other information, where eigenfrequencies and damping are indicated. A number of other parameters and plots are displayed, such as the auto-MAC matrix, mode complexity and animated mode shapes. The program tracks with every time step all the identified physical modes and can present the time evolution of modal parameters, by showing, for example, automatically the variation of damping and frequency over time during a flutter experiment. Almost all signal processing and identification parameters can be changed on-the-go by the user.
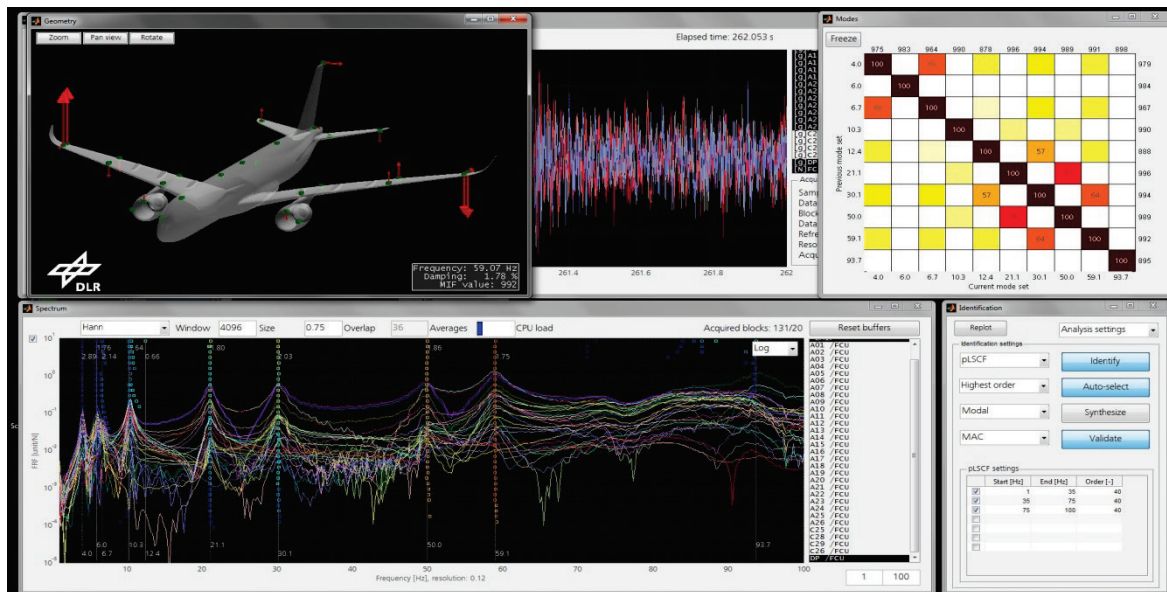

Figure 5: GUI in MATLAB of the automated system identification software (here with a transport aircraft model): animated mode shapes, time data, MAC matrix, spectrum and stabilization diagram, control panel.

4.2   Analysis

The random-like excitation from the turbulence in the flow is shown in Figure 6, where two examples of the online-recorded time response of the internal accelerometers are plotted. From $M_\infty = 0.5$ and $M_\infty = 0.74$ the response level is roughly doubled, then again at $M_\infty = 0.81$. Above $M_\infty = 0.82$ the system eventually becomes unstable. Figure 6, lower right, shows the diverging oscillations until the automatic flutter brake was triggered.
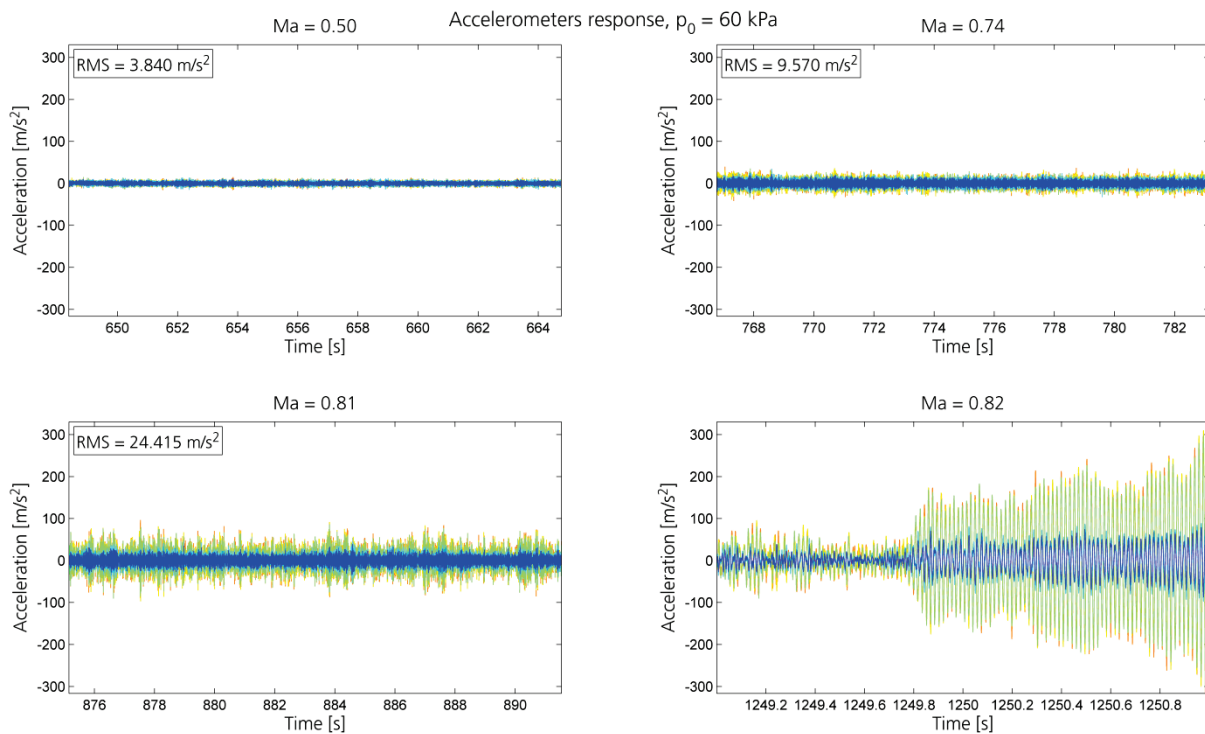

Figure 6: Time response of accelerometers and unstable condition

Figure 8 and Figure 9 display the frequencies and damping identified on-line for the heave and pitch mode over the Mach number. Each point on the graphs represents one identification elaborated from *65536* measured time data samples (all six accelerometers as references, Hann window, analysis band *5–85 Hz* *~400* frequency lines, model order *60*). The lines are average values and the 95% confidence interval in gray is calculated assuming a *t*-distribution of samples.

The frequency of the heave mode remains constant, but the frequency of the pitch mode is only constant till $M_\infty = 0.77$ before rising. This behavior can be explained with the rear loading effect of the airfoil at higher Mach numbers (see Figure 3), where the additional lift generated at oscillating angle of attack acts as a moment in opposite rotation to the angle. It appears as additional aerodynamic stiffness which results in increasing the eigenfrequency of the aeroelastic system. On the right side of Figure 8 the damping curves show significant scatter especially for lower Mach numbers, since in this range the excitation level of the turbulence is reduced, which results in a higher noise level of the acceleration response. The damping trend of the heave mode shows decreasing level up to $M_\infty = 0.77$ and then becomes more stable again. The behavior of the pitch mode is the other way around. The damping trend increases up to $M_\infty = 0.77$ and then slopes down to zero level, where self-excited flutter of the model occurs until the brake is activated triggered by the measured excessive deflection amplitudes.
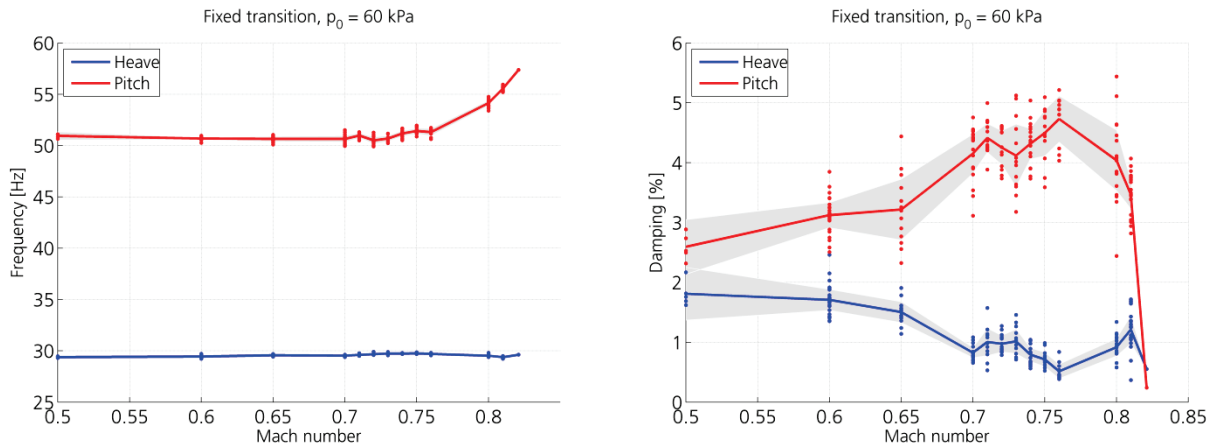
Figure 7: Frequency and damping of heave and pitch modes over Mach number

As an alternative to this very fast online modal identification method, an implementation of the Stochastic Subspace Identification is available in the monitoring software, which works in the time domain (see [1],[2],[3]). The data-driven version SSI-data uses directly the time blocks to fit a discrete time state space model, whereas the covariance-driven version SSI-cov analyses the impulse responses of the CPSDs, which are called cross correlation functions. The eigenvalues of the plant of the state space model are discrete poles, the corresponding mode shapes result from the output matrix. Finally, the poles must be transformed from discrete to continuous domain.
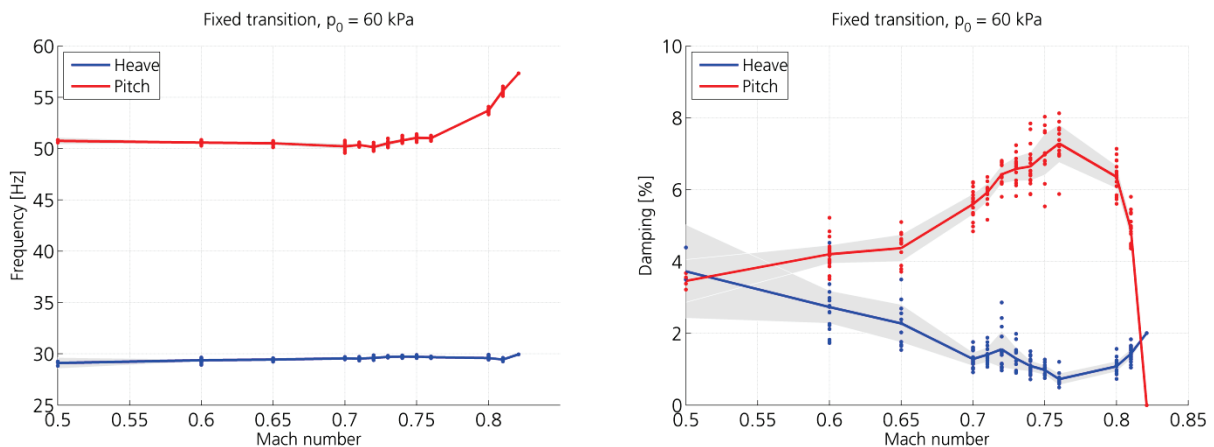

Figure 8: Frequency and damping of heave and pitch mode over Mach number with SSI-data method

In summary, this example demonstrates that the presented implementation of online automated operational modal analysis is suitable to monitor flutter experiments in wind tunnels.

5   Conclusions

The presented program for online-monitoring analysis (OMA) is based on a fast implementation of the well-known frequency-domain LSCF and pLSCF algorithms. Both are optimized for an almost real-time automated analysis of modal test sensor signals. Some insights about the different time complexities of both algorithms are given, highlighting parameters to which computation time is sensible. It is shown that a MATLAB implementation of the data processing and analysis program can be successfully utilized in the real-time monitoring an aeroelastic experiment in a wind-tunnel facility in combination with a commercial data acquisition hardware and software. The frequency and damping trends over Mach

number measured during a wind tunnel experiment of an instrumented airfoil model in the subsonic to transonic regimes are presented, including the onset of aeroelastic instabilities. The identified modal parameters are then compared with the results of a Stochastic Subspace Identification algorithm.

6   Outlook

For the assessment of the flutter stability the damping trends must be extrapolated towards higher speeds based on the identified dampings and frequencies at lower speeds. The method of Zimmerman and Weissenburger [19] predicts the critical speed of flutter onset by interpolating the identified poles with quadratic polynoms with at least three different speed points. It is assumed, that the unstable couplings is caused by contribution of only two mode shapes, one with heave character and the other with pitch character. In [20] this method is expanded to multimode unstable couplings, although the underlying assumption for the extrapolation is based on a constant aerodynamic lift and moment slope. The Zimmerman and Weissenburger method is therefore not applicable with adequate reliability.

The intended future work in monitoring aeroelastic experiments will include more sophisticated unsteady aerodynamic models for flutter prediction. In this framework, some possible developments are the use of half-power spectra as the primary data source, a fast maximum-likelihood estimator, delegation of intensive calculations to external code, different mode tracking algorithms.

Finally a future application will not only be monitoring of aeroelastic wind tunnel experiments but also flight flutter testing.

Acknowledgements

References

[1]   G. Dietz, G. Schewe, H. Mai: *Experiments on heave/pitch limit-cycle oscillations of a supercritical airfoil close to the transonic dip*, Journal of Fluids and Structures, 19 (2004), pp. 1–16.

[2]   G. Dietz, G. Schewe, H. Mai: *Amplifications and amplitude limitation of heave/pitch limit-cycle oscillations close to the transonic dip*, Journal of Fluids and Structures, 22 (2006), pp. 505–527.

[3]   A. De Vivo, C. Brutti, J.L. Leofanti: *Modal shape identification of large structure exposed to wind excitation by operational modal analysis technique*, Mechanical Systems and Signal Processing, Volume 39, Issues 1–2, August–September 2013, Pages 195-206, ISSN 0888-3270, **http://dx.doi.org/10.1016/j.ymssp.2013.03.025**.

[4]   J.M. Caicedo: *Practical guidelines for the natural excitation technique (next) and the eigensystem realiiation algorithm (ERA) for modal identification using ambient vibration*, Experimental Techniques July/August 2011.

[5]   P. van Overschee, B. De Moor: *Subspace Identification for Linear Systems*. Kluwer Academic Publishers, 1996.

[6]   J. Schoukens, Y. Rolain, F. Gustaffson, R. Pintelon: *Fast calculation of least-squares estimates for system identification*. Proceedings of the 32nd Decision and Control Conference, p. 3408-3410, Tampa, FL, USA, 1998.

[7]   B. Peeters, G. Lowet, H. van der Auweraer: *A new procedure for modal parameter estimation*, Sound and Vibration, January 2004.

[8]   B. Peeters, G. De Roeck: *Reference-based stochastic subspace identification for output-only modal analysis*. Mechanical Systems and Signal Processing, 13 (6) (1999), pp. 855–878.

[9]   E. Reynders, R. Pintelon, G. de Roeck: *Uncertainty bounds on modal parameters obtained from stochastic subspace identification*. Mechanical Systems and Signal Processing, Volume 22, Issue 4, May 2008, pp 948-969.

[10] M. Goursat, M. Doehler, L. Mevel, P. Andersen: *Crystal Clear SSI for Operational Modal Analysis of Aerospace Vehicles*, 28th International Modal Analysis Conference IMAC-XXVIII, 2010.

[11] R. Pintelon, J. Schoukens, *System identification – a frequency domain approach*, IEEE Press, 1st edition, 2001.

[12] E.J. Breitbach: *Recent Developments in Multiple Input Modal Analysis*, Journal of Vibration, Stress, and Reliability in Design, Vol. 110, pp. 478-484, 1988.

[13] W. Heylen, S. Lammens, P. Sas: *Modal Analysis Theory and Testing*, Seminar Notes of the Modal Analysis Seminar of the Katholieke Universiteit Leuven, Belgium, 2007, ISBN 90-73802-61-X.

[14] R. Pintelon, P. Guillaume, Y. Rolain, J. Schoukens, H. van Hamme: *Parametric identification of transfer functions in the frequency domain: a survey*. IEEE Transactrions on Automatic Control, 39(11):2245-2260, 1994.

[15] P. Verboven: *Frequency-domain system identification for modal analysis*. PhD thesis, Dept. of Mechanical Engineering, Vrije Universiteit Brussel, Belgium, 2002.

[16] B. Cauberghe: *Applied frequency-domain system identification in the field of experimental and operational modal analysis*. PhD thesis, Dept. of Mechanical Engineering, Vrije Universiteit Brussel, Belgium, 2004.

[17] G. H. Golub, C. F. van Loan: *Matrix computations*, third edition, Johns Hopkins University Press, 1996.

[18] N.N.: *DEWETRON, http://www.dewetron.com/applications/aerospace-defense/wind-tunnel-test/*

[19] N. H. Zimmerman, J. T. Weissenburger: *Prediction of Flutter Onset Speed Based on Flight Testing at Subcritical Speeds*, Journal of Aircraft, Vol.1 No.4 (1964), pp. 190–202.

[20] R. Lind: *Flutter Margins for Multimode Unstable Couplings with Associated Flutter Confidence,* Journal of Aircraft, Vol.46 No.45 (2009), pp. 1563–1569.